Science Advances
AAAS

Supplementary Materials for

Distinct roles for canonical and variant histone H3 lysine-36 in Polycomb silencing

Harmony R. Salzler *et al.*

Corresponding author: A. Gregory Matera, matera@unc.edu

Sci. Adv. **9**, eadf2451 (2023)
DOI: 10.1126/sciadv.adf2451

The PDF file includes:

Other Supplementary Material for this manuscript includes the following:

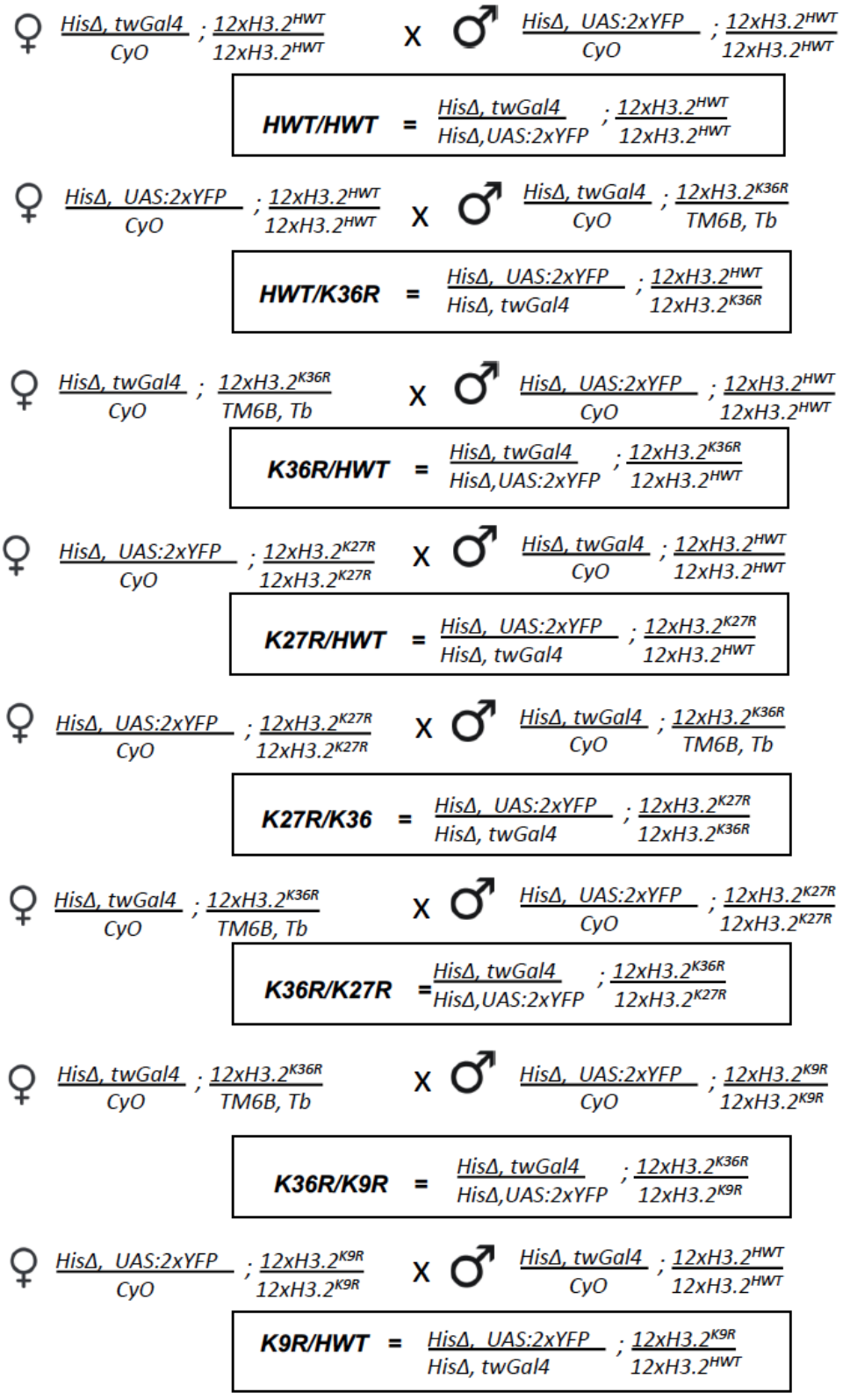

Fig. S1. Crossing Schemes to Generate Genotypes for Figure 1.
Crossing schemes used to generate the eight genotypes assayed in Figure 1B. Maternal and paternal genotypes are depicted above the boxes containing experimental genotypes. Experimental genotypes are indicated in both full and abbreviated forms.

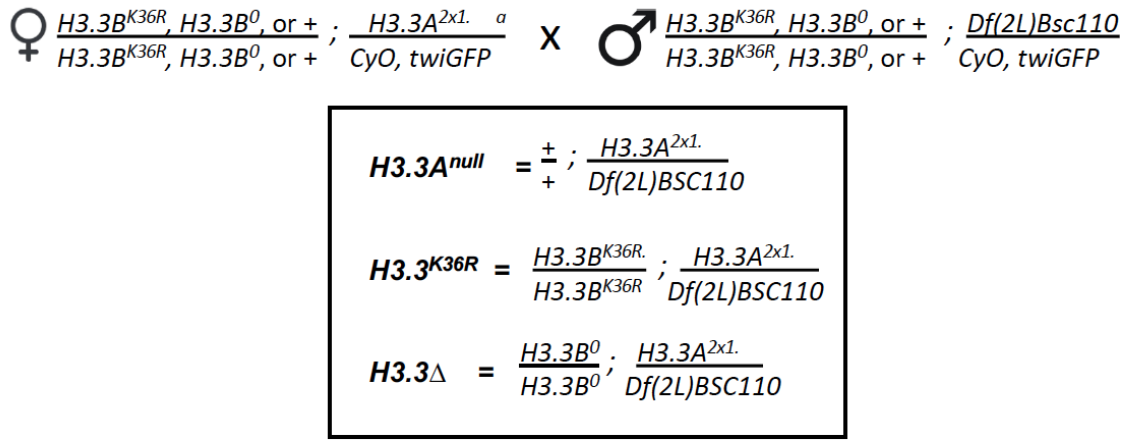

Fig. S2. Crossing Schemes to Generate Genotypes for Figure 2.
Crossing schemes used to generate 3 genotypes assayed in Figure 2A. Annotated as in Fig. S1. Note to obtain an *H3.3A*^{null} status for all, a deficiency (*Df(2L)BSC110)* was employed in trans to a null allele of *H3.3A*. Larvae were selected by GFP negative status.

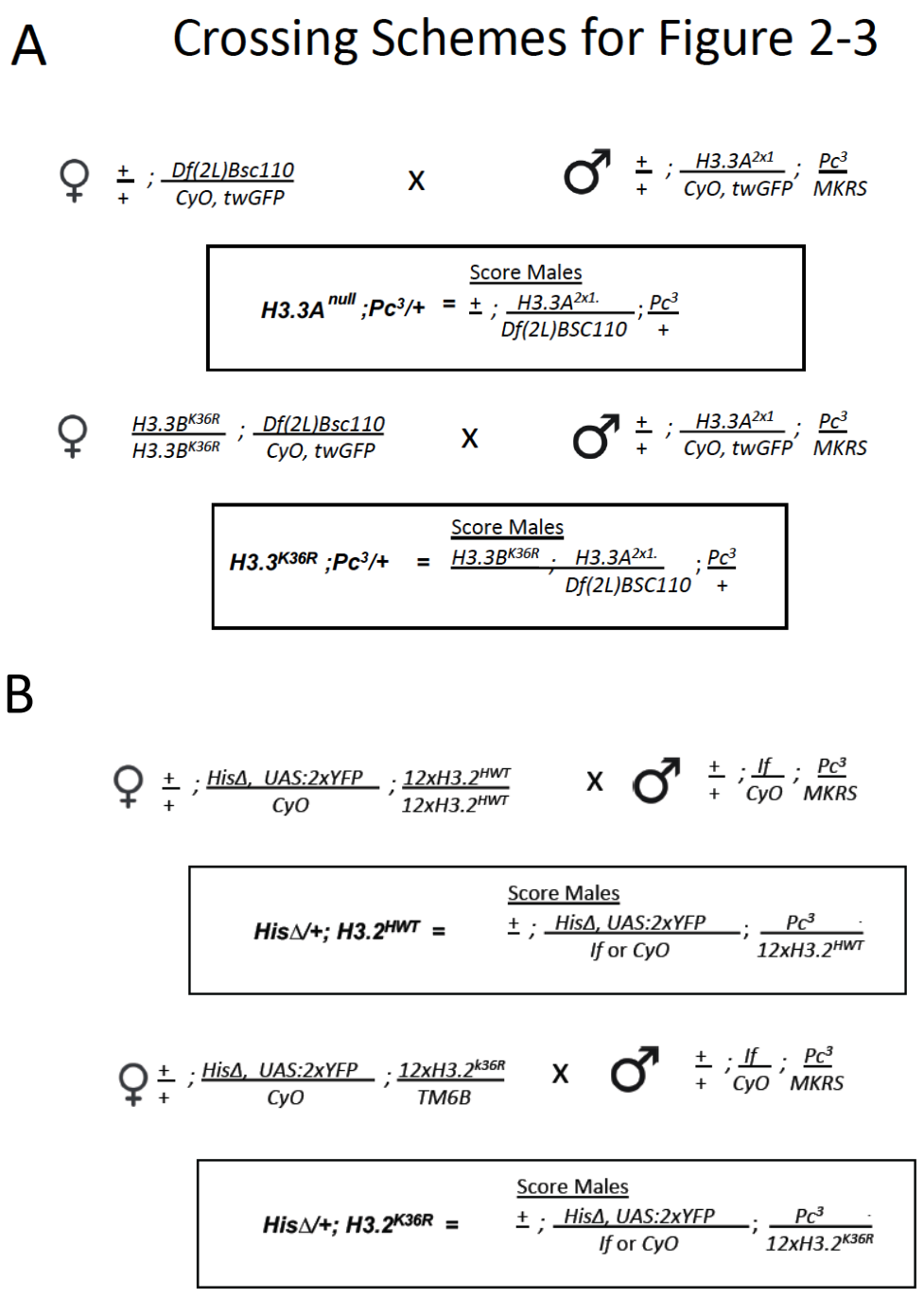

Fig. S3. Crossing Schemes to Generate Genotypes for Figures 2, 3, and S5. Crossing schemes used to generate 4 genotypes assayed in Figures 2, 3, and S5. Annotated as in Fig. S1. **(A)** Crosses pertaining to *H3.3*^{K26R} mutant and control. Note that the *HisC* locus is wild type. Experimental progeny were Cy and GFP negative. **(B)** Crosses pertaining to *H3.2*^{K26R} mutant and control. Note that both *If* and *CyO* offspring were scored.

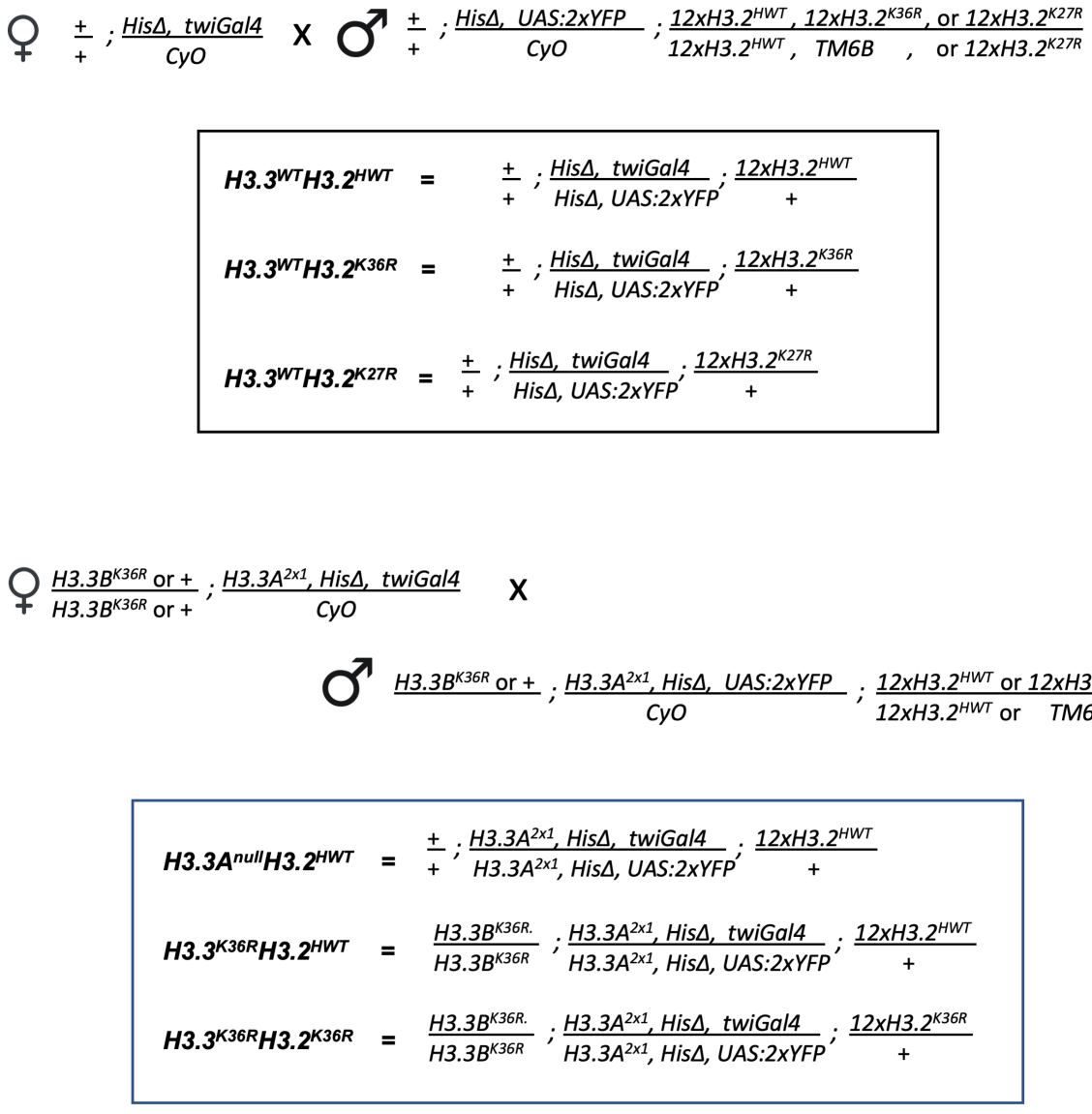

Fig. S4. Crossing Schemes to Generate Genotypes for Figures 4-7.
Crossing schemes used to generate 3 genotypes assayed in Figure 1B. Annotated as in Fig. S1. Note where applicable that to obtain an *H3.3A*^{null} status, the *H3.3A*^{2x1} allele is homozygous. All animals are in a *His*Δ plus 12x histone replacement transgenic background. Larvae were selected by YFP positive status.

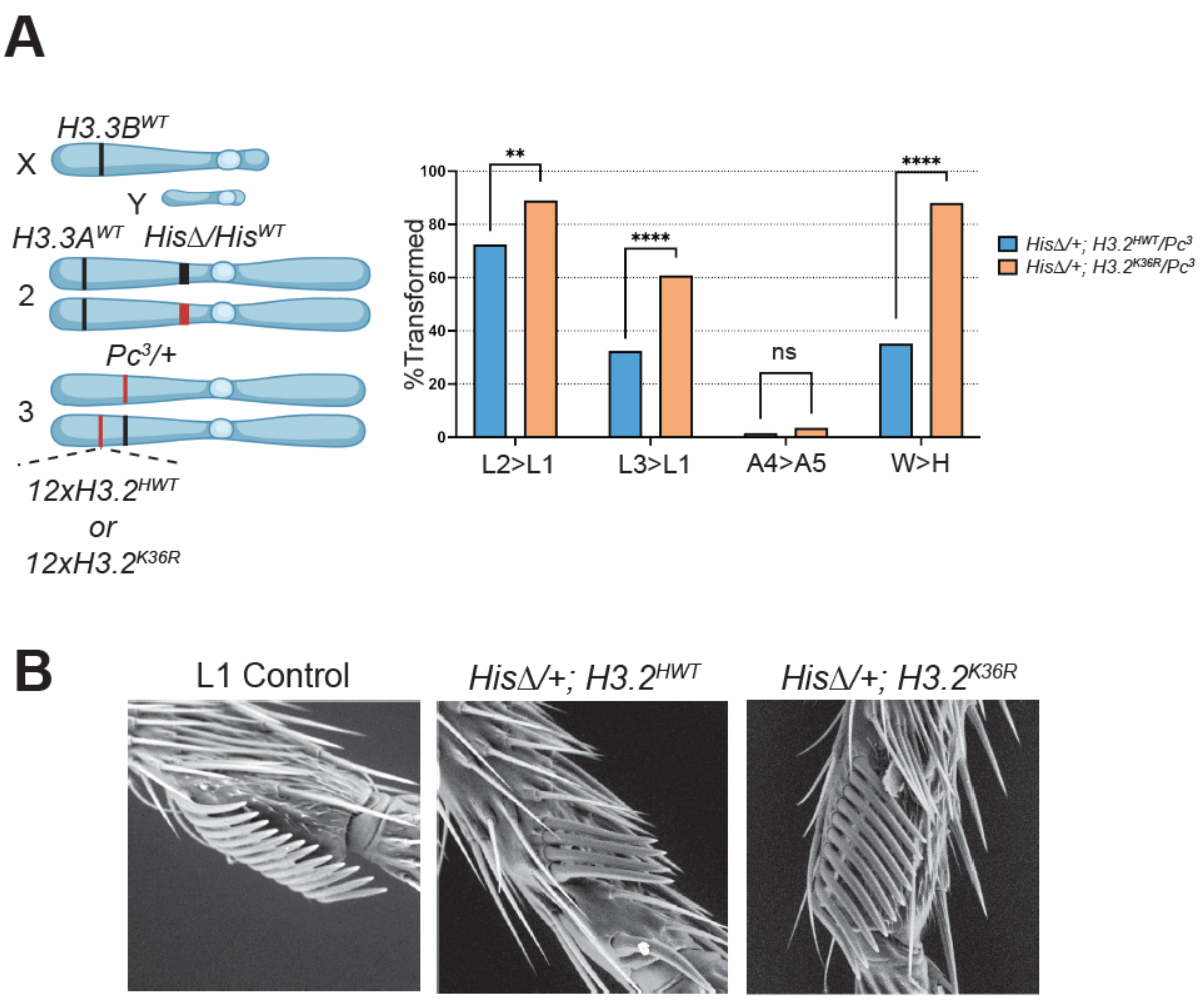

Fig. S5. Ectopic expression of *H3.2*^{K36R} Enhances Pc Transformations in Adults. Either *H3.2*^{K36R} and control histone genotypes were combined with a heterozygous Pc^3 mutation and scored for four characteristic PcG homeotic transformations. For full genetic scheme, see Fig. S2. T2-T1 (leg 2 to leg 1), T3-T1 (leg 3 to leg 4), A4-A5 (abdominal segment 4 to abdominal segment 5), and W-H (wing to haltere) transformations were scored for each genotype. Notably, for the *H3.2*^{K36R} analyses, the *HisC* locus was heterozygous to allow animals to reach adulthood, producing a ratio of *H3.2*^{WT} to *H3.2*^{K36R} genes of ~10:1 (endogenous *HisC* locus contains ~110 genes). **(A)** To the left, a summary of the genetic scheme for the *H3.2*^{K36R} and *Pc*^{3} genetic interaction experiment, created using BioRender.com. To the right, % Transformed for 4 homeotic transformations is plotted for each genotype. N value for number of flies scored for the *H3.2*^{K36R} genotype (n=55) and for the control (n=62). Note, for T2-T1 and T3-T1, each appendage was scored separately, effectively doubling the n value for these transformations. GraphPad Prism was used to calculate a χ^2 value for each transformation. Significance is abbreviated as: *=p<0.05, **=p<0.01, ***=p<0.001, ****=p<0.0001. **(B)** Image of a typical T2-T1 transformation for each genotype collected by scanning electron microscopy at 250x magnification.

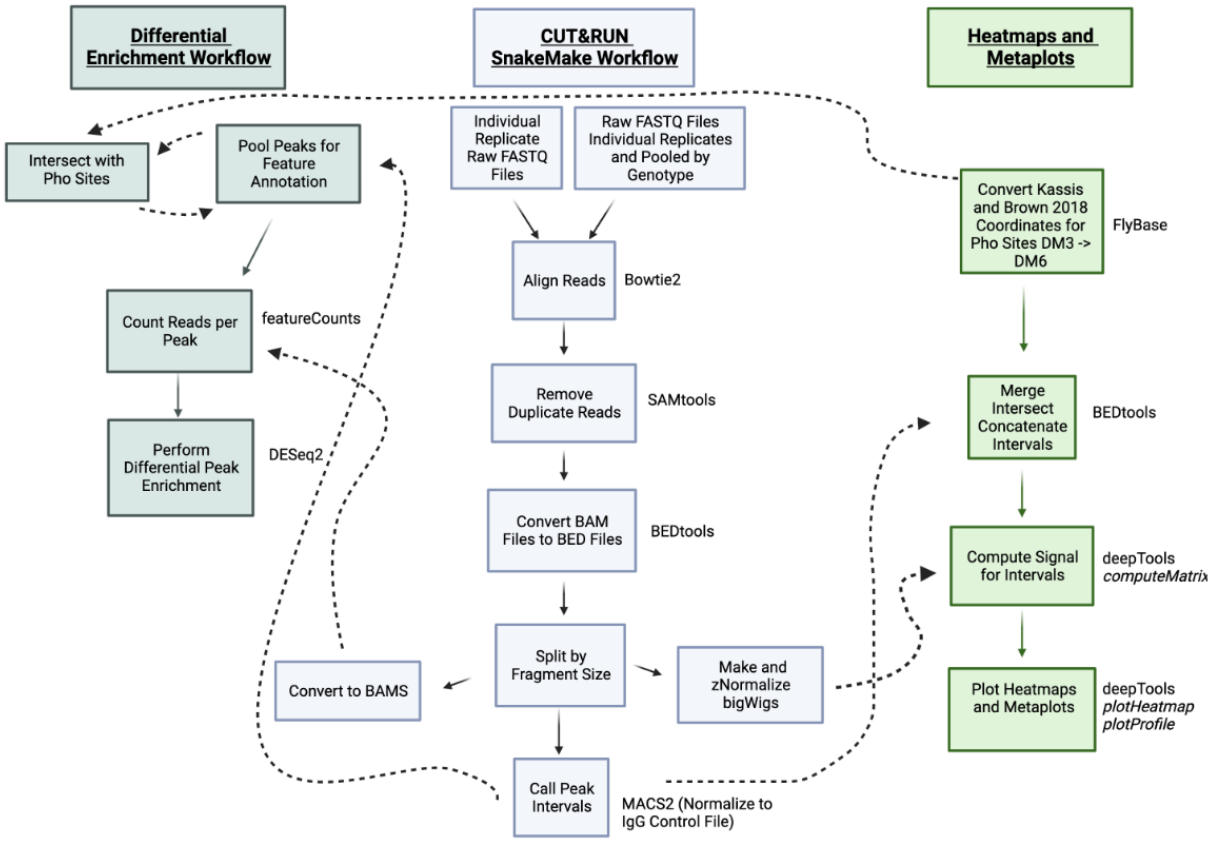

Fig. S6. Bioinformatic Workflow for CUT&RUN Analysis.
CUT&RUN data were processed as in https://github.com/mckaylabunc/cutNrun-pipeline with minor modifications. Briefly, QC was performed with FastQC (fastqc/0.11.7) *(114)* and FastQ Screen (v0.11.1) *(115)*. Reads were aligned with Bowtie2 (v2.3.4.1) *(116)* to the DM6 reference genome. SAMtools (v1.10) was used to remove duplicate reads and sort BAM files *(117)*. BAM files were converted to BED files using BEDTools (v2.26) *(113)*. These BED files were separated by fragment length (20-120bp, short fragments; 150-700bp, long fragments) and converted to separate fragment size binned BAM files. Bedgraphs were generated using BEDTools (v2.26) *(113)* and wigToBigWig *(118)* was used to convert BED files to bigWigs. BigWig files were RPGC (reads per genome coverage) normalized, and further transformed by z-normalization. Peak calling was performed using MACS2 (v2.1.2) *(119)* normalizing against an IgG control file.

Differential peak analysis was performed using featureCounts *(110)* and DESeq2 (v1.34.0) *(111)*. Details for generating intervals for each differential analysis (broad domains-Fig 4B, concatenated short fragment peaks from supernatant-Fig S11, short fragment peaks with Pho binding- Figs. 5C&S10B) can be found in Fig. S8. All genotypes were included to build each DESeq2 model. After models were created, differential analysis was performed between specified genotype comparisons of interest. For broad domains (Fig. 4B), pellet reads of all fragment sizes were used for DESeq2 analysis. For PRE based analyses in Fig 5C, S10B, and S11, only short fragment (20-120bp) pellet reads were analyzed with DESeq2.

All heatmaps and metaplots were generated from pooled bigWigs for each genotype using the deepTools (v3.2.0) package *(112)* and the reference-point option, rather than scale-region. Details for reference-point selection can be found in Fig. S8. Details for which files and parameters were used to produce heatmaps and metaplots can be found in the *Bioinformatic Analyses* section of Materials and Methods. This figure was created using BioRender.com.

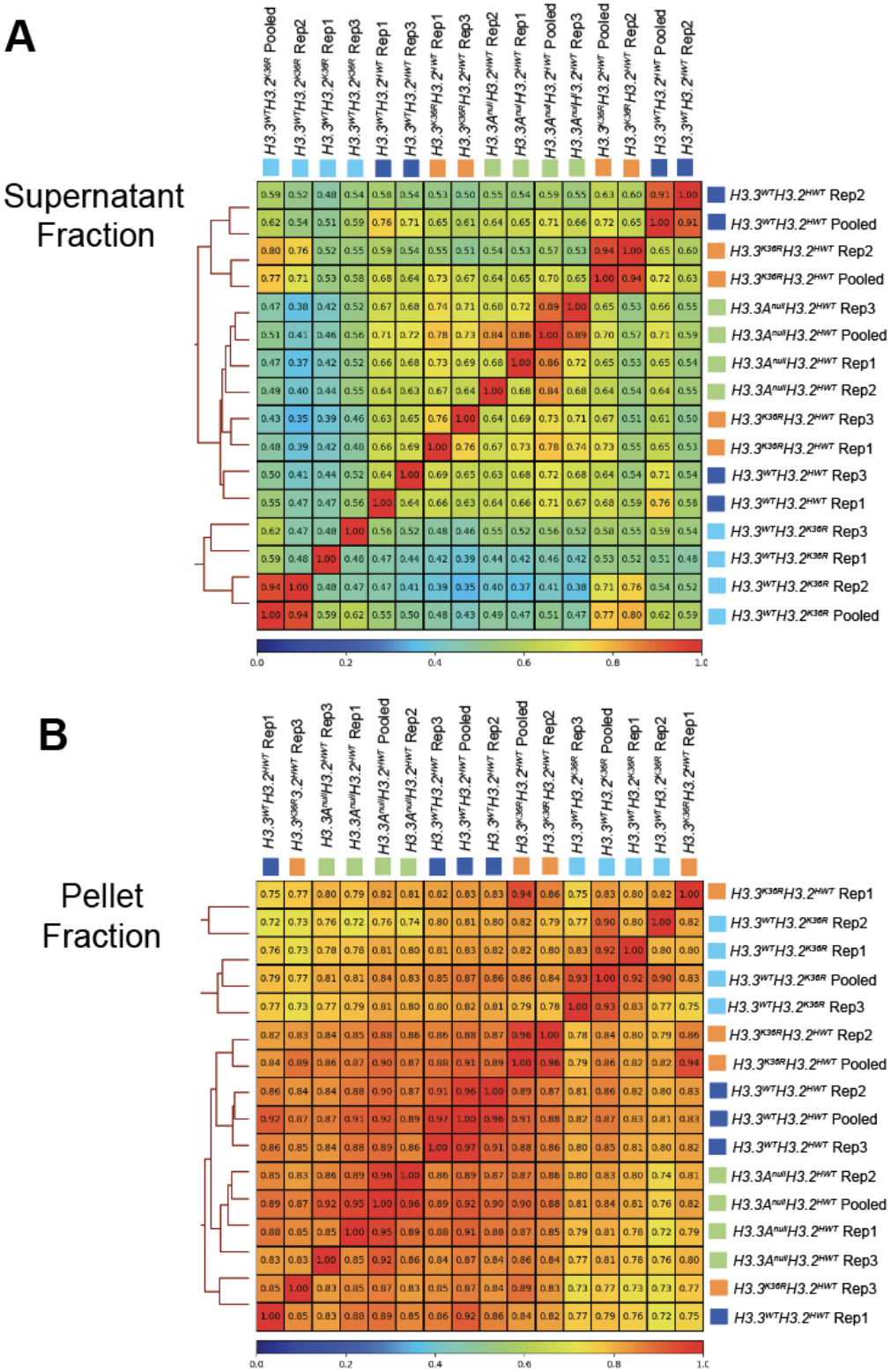

Fig. S7. Spearman Correlations for CUT&RUN Replicates
The deepTools (v3.5.1) package *(112)*, was used to calculate Spearman correlations between bigWig files from CUT&RUN replicates. **(A)** Supernatant fraction **(B)** Pellet fraction. Spearman correlations between replicates from the same genotype are higher from within the pellet fraction.

DESeq2 Interval Selection

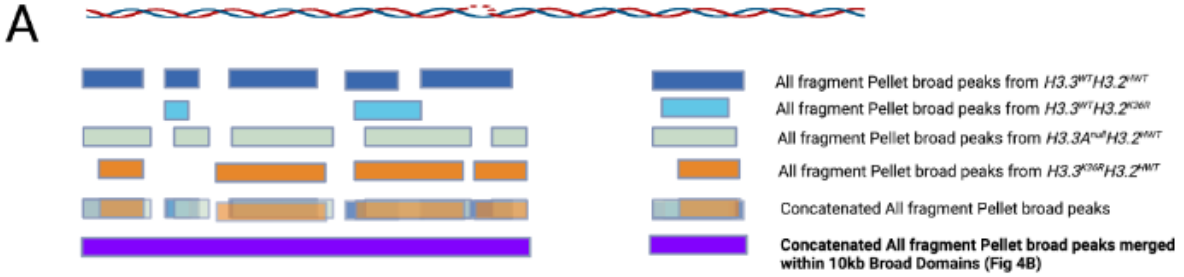

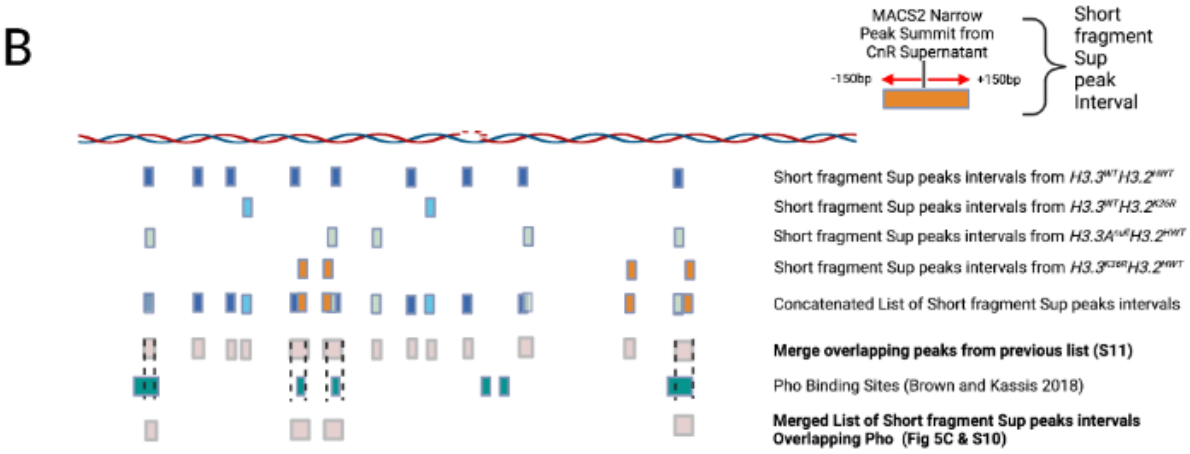

Heatmap and Metaplot Interval Selection

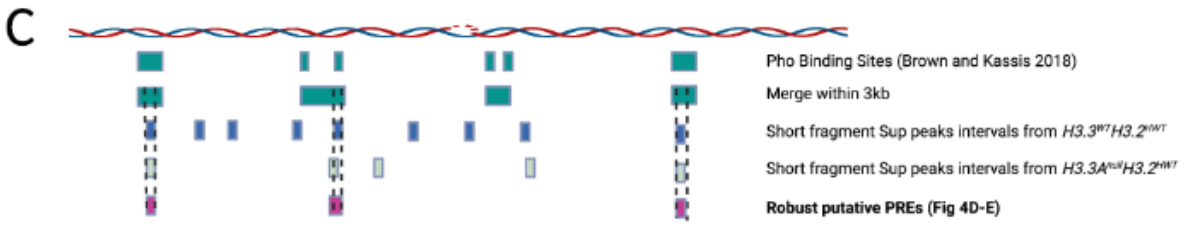

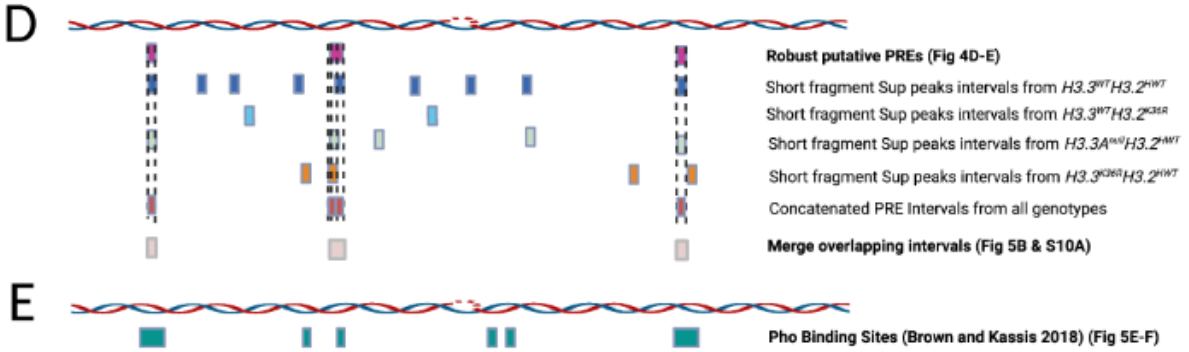

Fig. S8. Interval Selection for Bioinformatic Analyses.
BEDtools (v.2.3.0) *(109)* was used for intersecting and concatenating intervals from BED files generated from 1) Flybase Coordinate Converter Tool 2) MACS2 *(119)*. **(A)** For DESeq2 analysis of broad domains (Fig. 4B), broad peaks output by MACS2 for each genotype were concatenated with Bedtoolsr (2.30.0-4) *(120)*. Concatenated peaks were merged within 10kb to produce the broad domains used for the final analysis. **(B)** For narrow peak summit intervals in PRE analysis, short fragment supernatant narrow peak summits were extended +150bp. A master list concatenated from all four genotypes was further reduced by merging overlapping intervals, and used for the DESeq2 in analysis in Fig S11. For DESeq2 analyses of putative PRE regions with Pho binding capability, this list was intersected with Pho binding sites, and intervals overlapping Pho were analyzed in Fig 5C and S10B. **(C)** For heatmaps and metaplots in Fig4D-E, Pho binding regions from Brown and Kassis 2018 *(59)* were merged within 3kb with BEDTools (v.2.3.0). K27me3 MACS2 narrow peak summits + 150bp intervals from each control genotype that intersected these merged Pho intervals was compiled with BEDTools (v.2.3.0). Lists for both controls were intersected with BEDTools to generate a final list of "robust putative PREs" used for analysis in Fig. 4D. **(D)** For Figs. 5B & S10A metaplots, a master list of intervals from MACS2 narrow peak summits + 150bp for $H3.3^{WT}H3.2^{HWT}$, $H3.3^{WT}H3.2^{K36R}$, $H3.3A^{null}H3.2^{HWT}$, and $H3.3^{K36R}H3.2^{HWT}$ genotypes was concatenated. Overlapping intervals were merged. Merged intervals overlapping the "robust PREs" were used for subsequent metaplots. **(E)** For Figs. 5E-F, all unmerged Pho binding intervals *(59)* were sorted into 2 bed files by K27me3 status using the K27me3 broad domain peak annotation used for Fig. 4B with BEDTools (v.2.3.0). The Y chromosome was excluded for all analyses utilizing Pho binding data. This figure was created using BioRender.com.

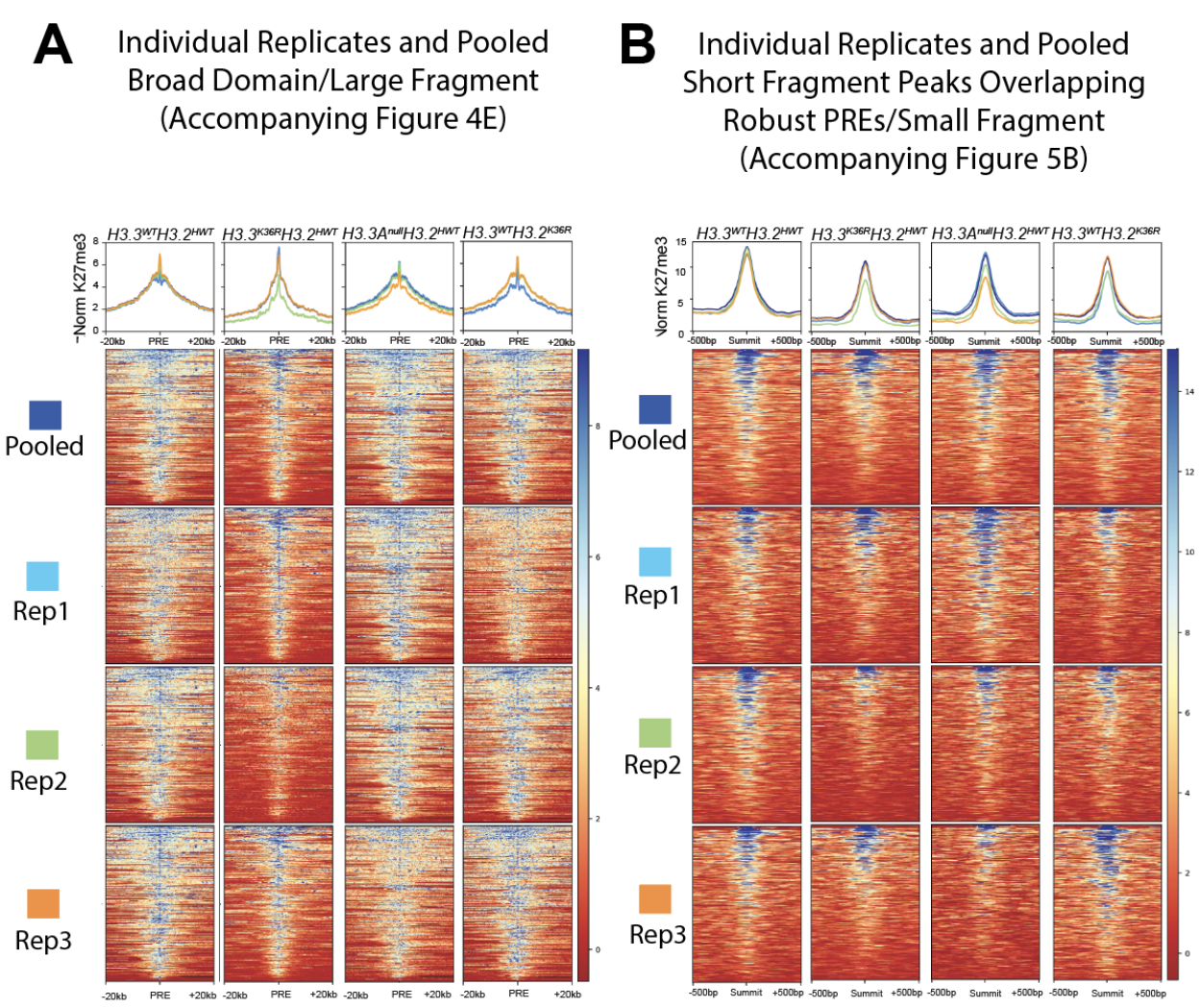

Fig. S9. Metaplots and Heatmaps for Individual CUT&RUN Replicates.
Analyses from Fig. 4E&5B were repeated with z-score normalized bigWigs from individual replicates alongside pooled bigWigs to assess the degree of variability between samples within the same genotype. **(A)** For broad domain analysis of large fragments, there is little variability between replicates, and pooled replicates overlay cleanly with the majority of individual replicates if one replicate is slightly lower. **(B)** Signal from short fragment pellet reads is generally more variable between replicates making precise quantification difficult.

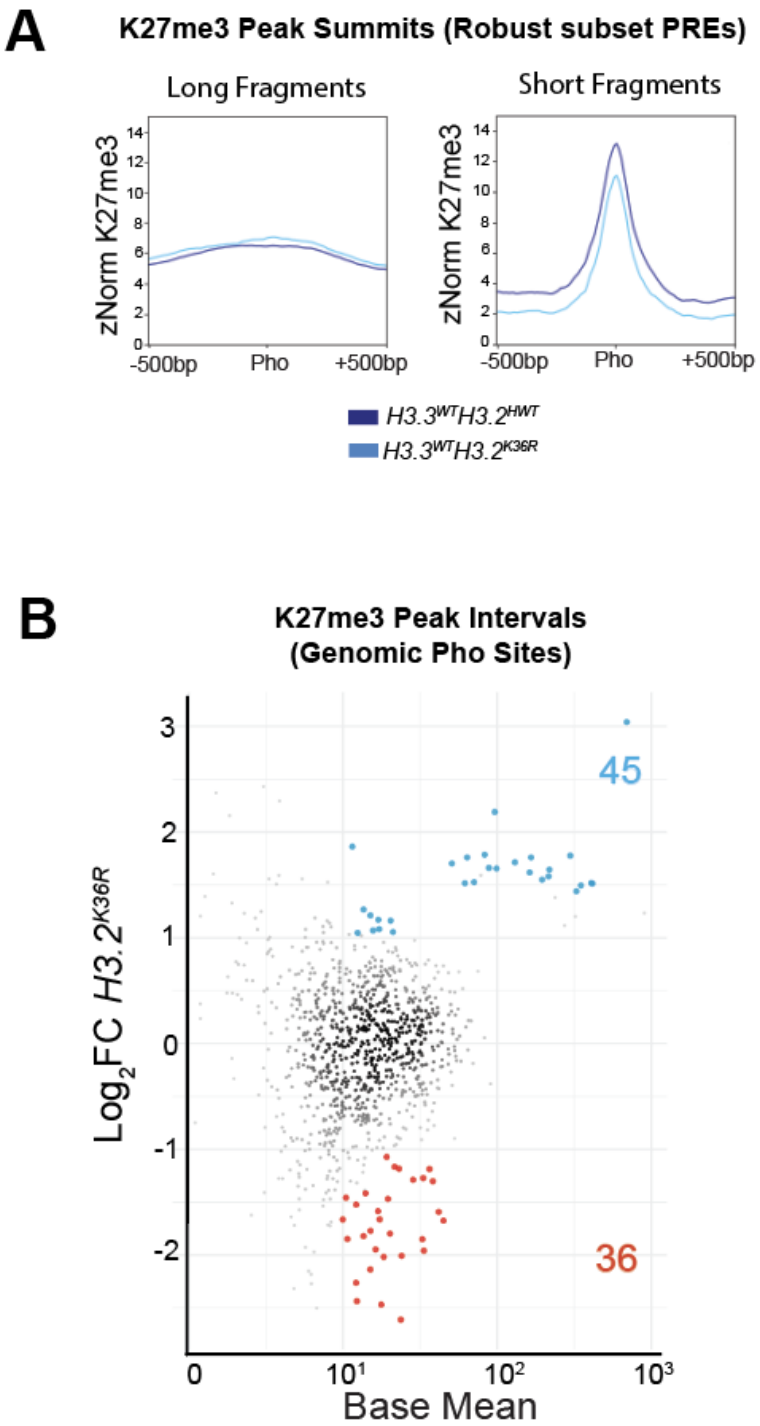

Fig. S10. H3K27me3 directed cleavage is unaltered at PREs in *H3.2*^{K36R} mutants. **(A)** Metaplots of K27me3 directed CUT&RUN signal + 500bp around peak summits called from all 4 genotypes that overlap robust PREs intervals identified in Figure 4 (n=426), see Fig. S8 for details. Separate plots were generated for long and short fragments. The *H3.3*^{WT}*H3.2*^{K36R} mutant is plotted alongside the *H3.3*^{WT}*H3.2*^{HWT} control. **(B)** DESeq2 analysis for peak summit intervals identified from all 4 genotypes overlapping Kassis Pho binding sites genome-wide (n=985) for the *H3.3*^{K36R}*H3.2*^{HWT} mutant vs. control, annotated as in Fig 5B.

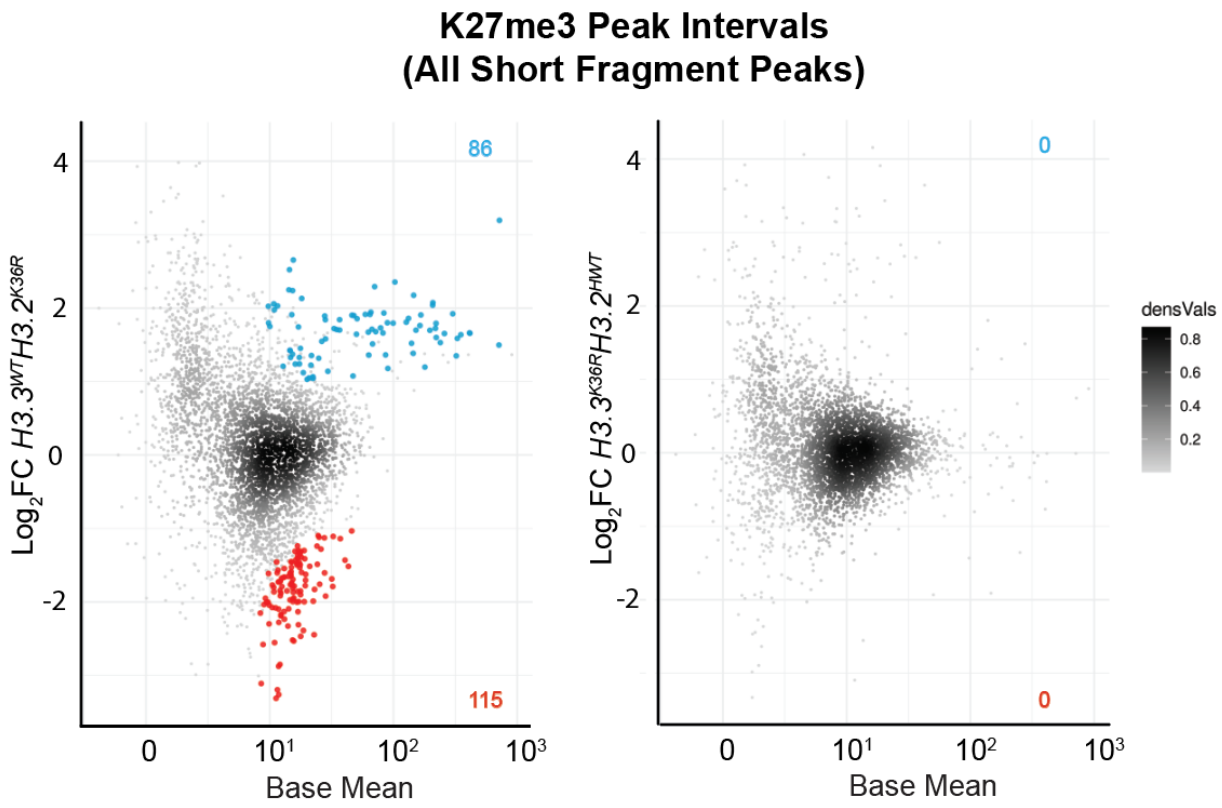

Fig. S11. Differential Peak Analysis of All H3K27me3 Subnucleosomal Fragment Sized Peaks. DESeq2 differential analysis of all H3K27me3 short fragment peak summit intervals , irrespective of Pho status (n=4341). An M/A plot of these intervals for 1) *H3.3*^{WT}*H3.2*^{K36R} mutant vs. *H3.3*^{WT}*H3.2*^{HWT} control and 2) *H3.3*^{K36R}*H3.2*^{HWT} mutant vs. *H3.3A*^{null}*H3.2*^{HWT} control is shown (details in Fig. S8). Points with an adjusted p-value > 0.05 and a Log_2 fold change (Log_2FC) > |1| are colored (red = downregulated, blue = upregulated).

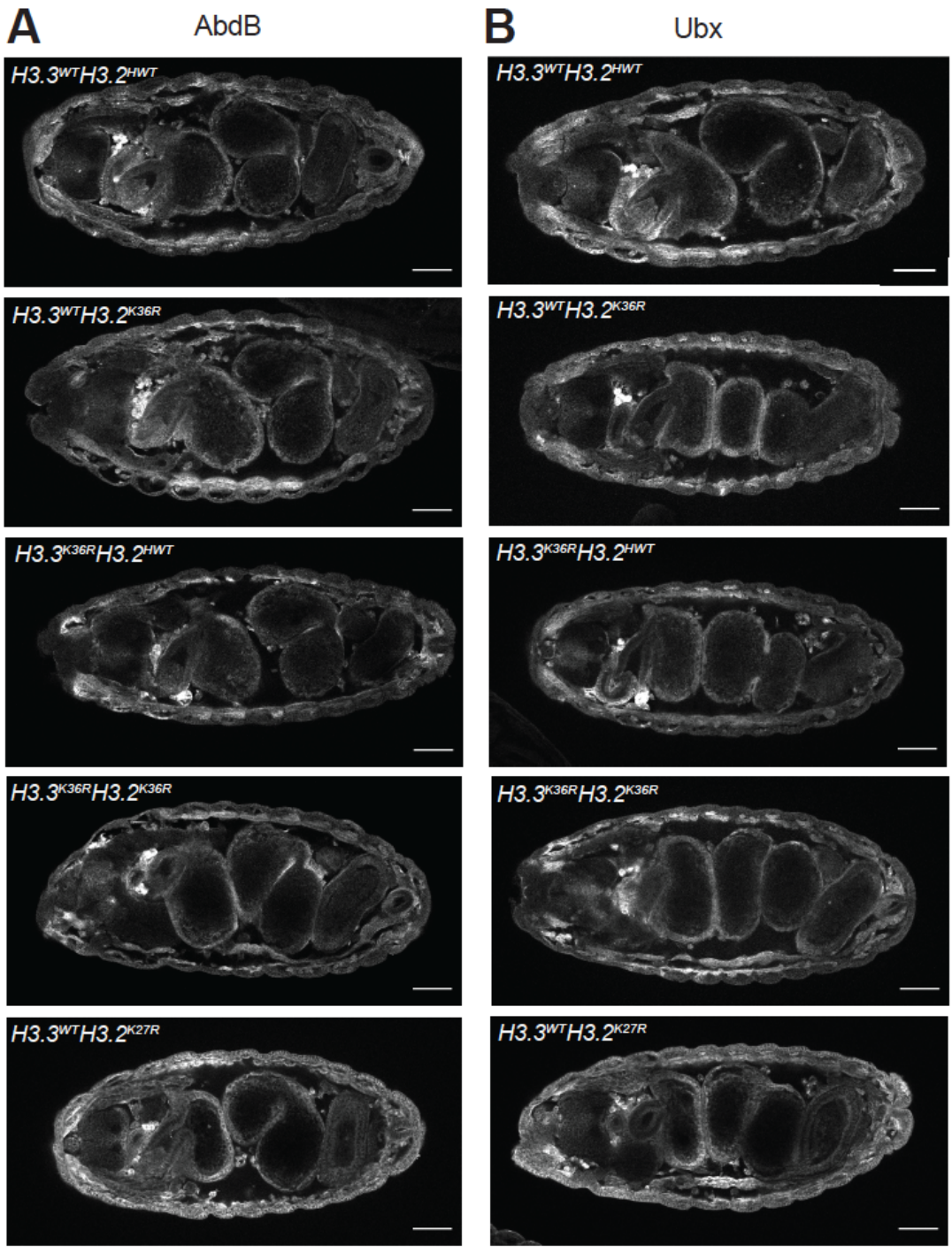

Fig. S12. Images Used for Staging Embryos in Figure 3.
(A) Stage 16 embryos of H3K36R mutant genotypes and controls were fixed and stained with anti-AbdB antibodies. Embryos were stained with anti-GFP antibodies to detect YFP for staging and genotype selection. For each embryo, a single slice from the anti-GFP channel was used for staging the embryos in Figure 3A. Scale bar = 50μm. **(B)** Same as in A, except staging for embryos stained with anti-Ubx instead of anti-AbdB, and from the embryos depicted in Figure 3B.

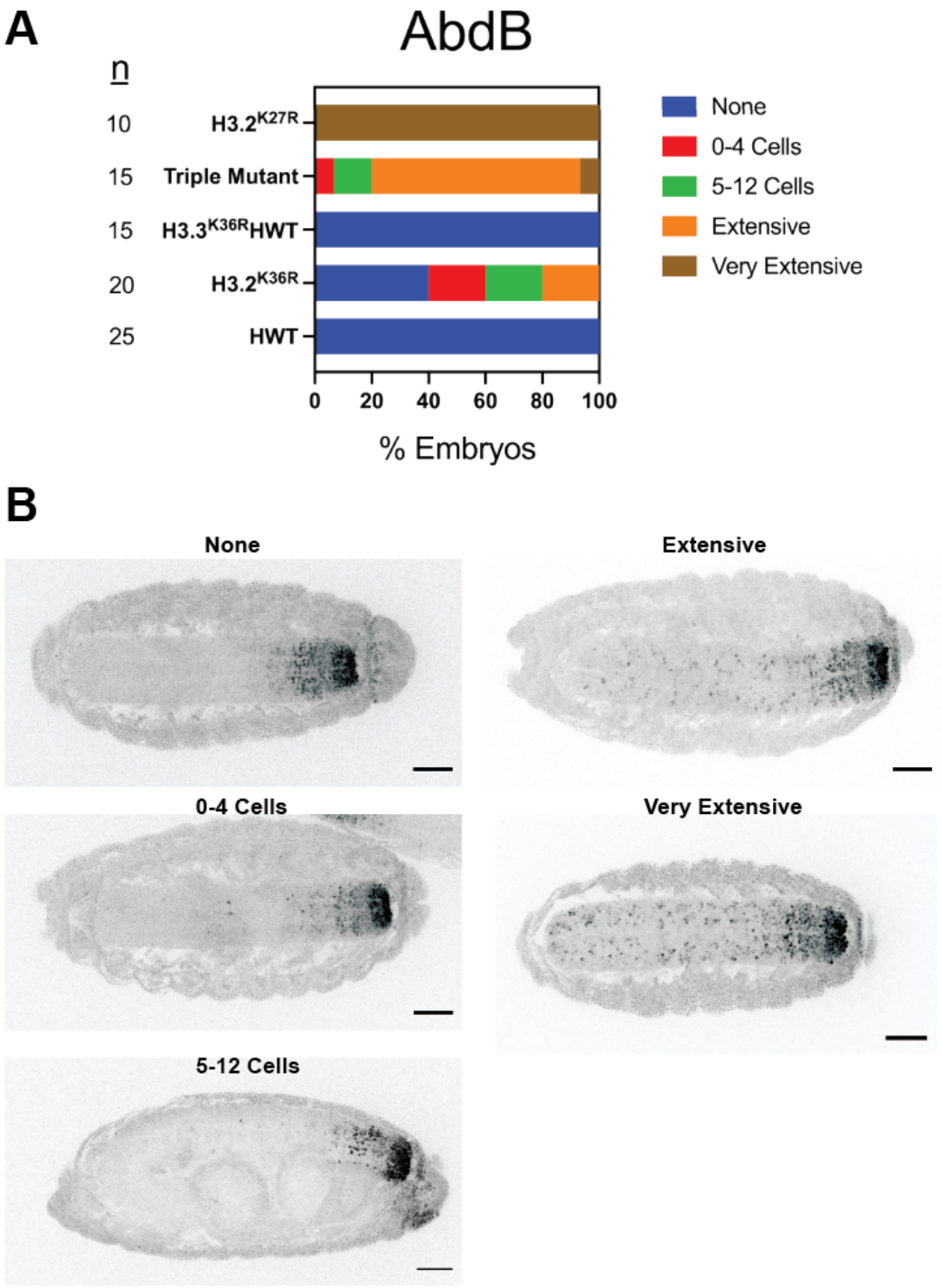

Fig. S13. Classification of AbdB derepression phenotypes in Stage 16 embryos. **(A)** Stage 16 embryos were stained for AbdB, and maximum intensity Z-projections through the VNC were created and inspected for derepressed cells (see Fig.7 and methods for details). A horizontally stacked bar graph indicates percentages of each genotype falling into each category of phenotypic severity. For each genotype an n (left of graph) indicates the number of stage 16 embryos subjected to detailed image analysis . **(B)** Example images of stage 16 embryos falling into each category examined in A.

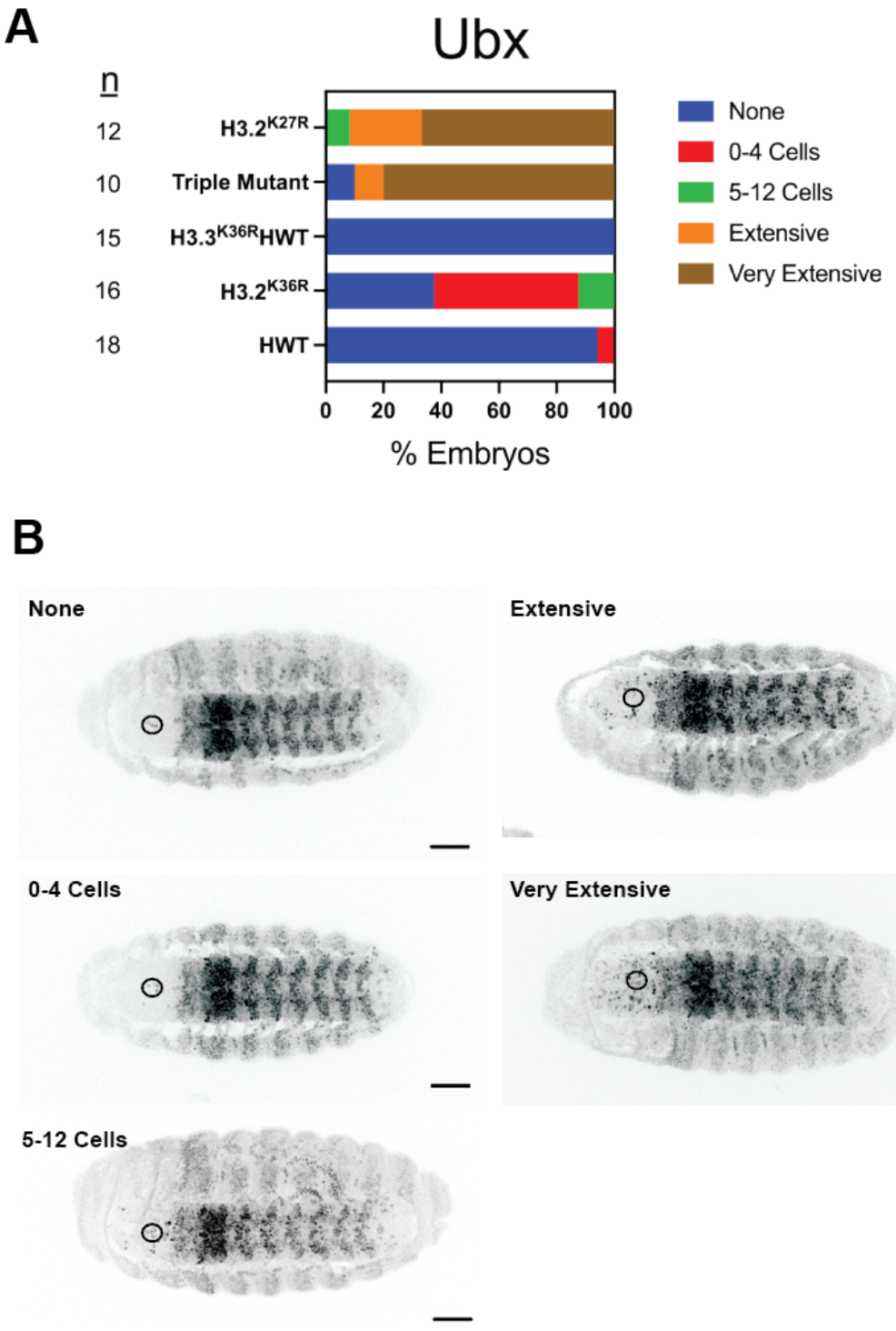

Fig. S14. Classification of Ubx derepression phenotypes in Stage 16 embryos. (A) Stage 16 embryos were stained for Ubx and maximum intensity Z-projections through the VNC were created and inspected for derepressed cells (see Fig.7 and methods for details). A horizontally stacked bar graph indicates percentages of each genotype falling into each category of phenotypic severity. For each genotype an n (left of graph) indicates the number of stage 16 embryos subjected to detailed image analysis . **(B)** Example images of stage 16 embryos falling into each category examined in A. Black circles indicate cells excluded from consideration because we observed Ubx expression in control embryos.

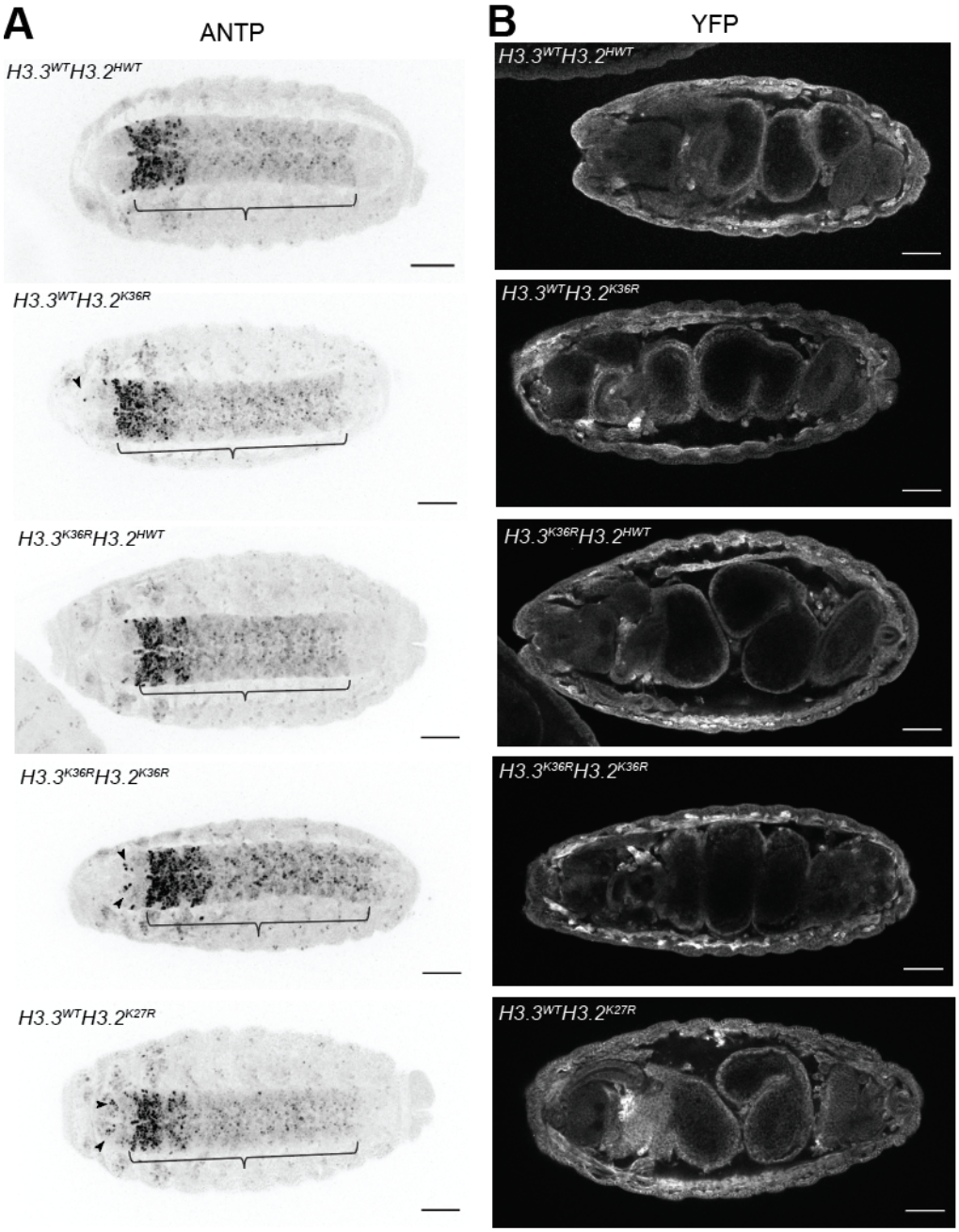

Fig. S15. Embryos with Combined Mutation of *H3.3*^{K36R} and *H3.2*^{K36R} Exhibit Moderate Synergistic Derepression of ANTP. Stage 16 embryos of H3K36R mutant genotypes and controls were fixed and stained with anti-ANTP antibodies. Embryos were stained with anti-GFP antibodies to detect YFP for staging and genotype selection. Scale bar = 50μm. **(A)** Representative Anti-ANTP staining for 5 genotypes. Brackets indicate the expected boundary of ANTP expression in wild type embryos. Filled arrows highlight individual cells exhibiting anterior derepression of ANTP. Black arrows indicate derepressed cells. Overall, individual H3.2 and H3.3 mutants closely resemble *H3.3*^{WT}*H3.2*^{HWT} negative controls, while *H3.3*^{K36R}*H3.2*^{K36R} were generally intermediate between *H3.3*^{WT}*H3.2*^{HWT} and *H3.3*^{WT}*H3.2*^{K27R} controls. **(B)** Single slice from anti-GFP channel staining YFP for same embryos in A depicting staging.

Nomenclature	Genotype
For Figure 1A	
HWT/HWT	$\frac{HisΔ,\ twiGal4}{HisΔ,\ UAS:YFP}; \frac{12xH3.2^{HWT}}{12xH3.2^{HWT}}$
HWT/K36R	$\frac{HisΔ,\ twiGal4}{HisΔ,\ UAS:YFP}; \frac{12xH3.2^{HWT}}{12xH3.2^{K36R}}$
K36R/HWT	$\frac{HisΔ,\ twiGal4}{HisΔ,\ UAS:YFP}; \frac{12xH3.2^{K36R}}{12xH3.2^{HWT}}$
K36R/K27R	$\frac{HisΔ,\ twiGal4}{HisΔ,\ UAS:YFP}; \frac{12xH3.2^{K36R}}{12xH3.2^{K27R}}$
K36R/K9R	$\frac{HisΔ,\ twiGal4}{HisΔ,\ UAS:YFP}; \frac{12xH3.2^{K36R}}{12xH3.2^{K9R}}$
K27R/K36R	$\frac{HisΔ,\ twiGal4}{HisΔ,\ UAS:YFP}; \frac{12xH3.2^{K27R}}{12xH3.2^{K36R}}$
K27R/HWT	$\frac{HisΔ,\ twiGal4}{HisΔ,\ UAS:YFP}; \frac{12xH3.2^{K36R}}{12xH3.2^{HWT}}$
K9R/HWT	$\frac{HisΔ,\ twiGal4}{HisΔ,\ UAS:YFP}; \frac{12xH3.2^{K9R}}{12xH3.2^{HWT}}$
For Figures 1B, and 4-7	
$H3.3A^{null}$	$\frac{+}{+}; \frac{H3.3A^{2x1}}{Df(2L)Bsc110}; \frac{+}{+}$
$H3.3^{K36R}$	$\frac{H3.3B^{K36R}}{H3.3B^{K36R}}; \frac{H3.3A^{2x1}}{Df(2L)Bsc110}; \frac{+}{+}$
H3.3Δ	$\frac{H3.3B^{0}}{H3.3B^{0}}; \frac{H3.3A^{2x1}}{Df(2L)Bsc110}; \frac{+}{+}$
$H3.3^{WT}H3.2^{HWT}$	$\frac{+}{+}; \frac{HisΔ,\ twiGal4}{HisΔ,\ UAS:YFP}; \frac{12xH3.2^{HWT}}{+}$
$H3.3^{WT}H3.2^{K36R}$	$\frac{+}{+}; \frac{HisΔ,\ twiGal4}{HisΔ,\ UAS:YFP}; \frac{12xH3.2^{K36R}}{+}$
$H3.3^{null}H3.2^{HWT}$	$\frac{+}{+}; \frac{H3.3A^{2x1},\ HisΔ,\ twiGal4}{H3.3A^{2x1},\ HisΔ,\ UAS:YFP}; \frac{12xH3.2^{HWT}}{+}$
$H3.3^{K36R}H3.2^{HWT}$	$\frac{H3.3B^{K36R}}{H3.3B^{K36R}}; \frac{H3.3A^{2x1},\ HisΔ,\ twiGal4}{H3.3A^{2x1},\ HisΔ,\ UAS:YFP}; \frac{12xH3.2^{HWT}}{+}$
$H3.3^{K36R}H3.2^{K36R}$	$\frac{H3.3B^{K36R}}{H3.3B^{K36R}}; \frac{H3.3A^{2x1},\ HisΔ,\ twiGal4}{H3.3A^{2x1},\ HisΔ,\ UAS:YFP}; \frac{12xH3.2^{K36R}}{+}$
$H3.3^{WT}H3.2^{K27R}$	$\frac{+}{+}; \frac{HisΔ,\ twiGal4}{HisΔ,\ UAS:YFP}; \frac{12xH3.2^{K27R}}{+}$

Table S1. Shorthand nomenclature for genotypes used in this study.
A key is provided here for easy reference. The left column indicates the shorthand genotype used in the text and figures. The right column lists the full genotype with all relevant alleles and transgenes.

Table S2. DESeq2 Output for K27me3 CUT&RUN for Broad Domains. DESeq2 output accompanying Fig. 4B. Differential peak analysis by DESeq2 on broad H3K27me3 domains (details in Fig.S8) using all-fragment BAM files from the pellet fraction. Separate columns comparing $H3.3^{WT}H3.2^{K36R}$ vs. $H3.3^{WT}H3.2^{HWT}$ control and $H3.3^{K36R}H3.2^{HWT}$ vs. $H3.3A^{null}H3.2^{HWT}$ are included.

Table S3. DESeq2 Output for K27me3 CUT&RUN for Short Fragment Peak Intervals Overlapping Pho. DESeq2 output accompanying Fig. 5C and S10B. Differential peak analysis by DESeq2 on short fragment peak intervals from H3K27me3 domains CUT&RUN that overlap Pho binding sites (details in Fig.S8) using small fragment BAM files from the pellet fraction. Separate columns comparing $H3.3^{WT}H3.2^{K36R}$ vs. $H3.3^{WT}H3.2^{HWT}$ control and $H3.3^{K36R}H3.2^{HWT}$ vs. $H3.3A^{null}H3.2^{HWT}$ are included.

Table S4. DESeq2 Output for All K27me3 CUT&RUN for Short Fragment Peak Intervals. DESeq2 output accompanying Fig. S11. Differential peak analysis by DESeq2 on short fragment peak intervals from H3K27me3 domains CUT&RUN (details in Fig.S8) using small fragment BAM files from the pellet fraction. Separate columns comparing $H3.3^{WT}H3.2^{K36R}$ vs. $H3.3^{WT}H3.2^{HWT}$ control and $H3.3^{K36R}H3.2^{HWT}$ vs. $H3.3A^{null}H3.2^{HWT}$ are included.

REFERENCES AND NOTES

1. N. Camacho-Ordonez, E. Ballestar, H. T. M. Timmers, B. Grimbacher, What can clinical immunology learn from inborn errors of epigenetic regulators? *J. Allergy Clin. Immunol.* **147**, 1602–1618 (2021).

2. E. Conway, E. Healy, A. P. Bracken, PRC2 mediated H3K27 methylations in cellular identity and cancer. *Curr. Opin. Cell Biol.* **37**, 42–48 (2015).

3. J. H. Lee, J.-H. Kim, S. Kim, K. S. Cho, S. B. Lee, Chromatin changes associated with neuronal maintenance and their pharmacological application. *Curr. Neuropharmacol.* **16**, 118–125 (2018).

4. A. Piunti, A. Shilatifard, The roles of Polycomb repressive complexes in mammalian development and cancer. *Nat. Rev. Mol. Cell Biol.* **22**, 326–345 (2021).

5. A. Elsherbiny, G. Dobreva, Epigenetic memory of cell fate commitment. *Curr. Opin. Cell Biol.* **69**, 80–87 (2021).

6. J.-Y. Hwang, K. A. Aromolaran, R. S. Zukin, The emerging field of epigenetics in neurodegeneration and neuroprotection. *Nat. Rev. Neurosci.* **18**, 347–361 (2017).

7. K. R. Stewart-Morgan, N. Petryk, A. Groth, Chromatin replication and epigenetic cell memory. *Nat. Cell Biol.* **22**, 361–371 (2020).

8. B. D. Strahl, C. D. Allis, The language of covalent histone modifications. *Nature* **403**, 41–45 (2000).

9. D. J. McKay, S. Klusza, T. J. Penke, M. P. Meers, K. P. Curry, S. L. McDaniel, P. Y. Malek, S. W. Cooper, D. C. Tatomer, J. D. Lieb, B. D. Strahl, R. J. Duronio, A. G. Matera, Interrogating the function of metazoan histones using engineered gene clusters. *Dev. Cell* **32**, 373–386 (2015).

10. M. P. Meers, M. Leatham-Jensen, T. J. R. Penke, D. J. McKay, R. J. Duronio, A. G. Matera, An animal model for genetic analysis of multi-gene families: Cloning and transgenesis of large tandemly repeated histone gene clusters. *Methods Mol. Biol.* **1832**, 309–325 (2018).

11. R. L. Armstrong, T. J. R. Penke, B. D. Strahl, A. G. Matera, D. J. McKay, D. M. MacAlpine, R. J. Duronio, Chromatin conformation and transcriptional activity are permissive regulators of DNA replication initiation in Drosophila. *Genome Res.* **28**, 1688–1700 (2018).

12. M. P. Meers, T. Henriques, C. A. Lavender, D. J. McKay, B. D. Strahl, R. J. Duronio, K. Adelman, A. G. Matera, Histone gene replacement reveals a post-transcriptional role for H3K36 in maintaining metazoan transcriptome fidelity. *eLife* **6**, e23249 (2017).

13. T. J. Penke, D. J. McKay, B. D. Strahl, A. G. Matera, R. J. Duronio, Direct interrogation of the role of H3K9 in metazoan heterochromatin function. *Genes Dev.* **30**, 1866–1880 (2016).

14. T. J. R. Penke, D. J. McKay, B. D. Strahl, A. G. Matera, R. J. Duronio, Functional redundancy of variant and canonical histone H3 lysine 9 modification in drosophila. *Genetics* **208**, 229–244 (2018).

15. B. Schuettengruber, H. M. Bourbon, L. Di Croce, G. Cavalli, Genome regulation by polycomb and trithorax: 70 years and counting. *Cell* **171**, 34–57 (2017).

16. J. A. Simon, R. E. Kingston, Occupying chromatin: Polycomb mechanisms for getting to genomic targets, stopping transcriptional traffic, and staying put. *Mol. Cell* **49**, 808–824 (2013).

17. R. T. Coleman, G. Struhl, Causal role for inheritance of H3K27me3 in maintaining the OFF state of a *Drosophila* HOX gene. *Science* **356**, eaai8236 (2017).

18. A. R. Pengelly, Ö. Copur, H. Jäckle, A. Herzig, J. Müller, A histone mutant reproduces the phenotype caused by loss of histone-modifying factor Polycomb. *Science* **339**, 698–699 (2013).

19. K. H. Hansen, A. P. Bracken, D. Pasini, N. Dietrich, S. S. Gehani, A. Monrad, J. Rappsilber, M. Lerdrup, K. Helin, A model for transmission of the H3K27me3 epigenetic mark. *Nat. Cell Biol.* **10**, 1291–1300 (2008).

20. L. Jiao, X. Liu, Structural basis of histone H3K27 trimethylation by an active polycomb repressive complex 2. *Science* **350**, aac4383-aac4383 (2015).

21. R. Margueron, N. Justin, K. Ohno, M. L. Sharpe, J. Son, W. J. Drury III, P. Voigt, S. R. Martin, W. R. Taylor, V. De Marco, V. Pirrotta, D. Reinberg, S. J. Gamblin, Role of the polycomb protein EED in the propagation of repressive histone marks. *Nature* **461**, 762–767 (2009).

22. M. Uckelmann, C. Davidovich, Not just a writer: PRC2 as a chromatin reader. *Biochem. Soc. Trans.* **49**, 1159–1170 (2021).

23. T. Zhang, S. Cooper, N. Brockdorff, The interplay of histone modifications - writers that read. *EMBO Rep.* **16**, 1467–1481 (2015).

24. N. P. Blackledge, R. J. Klose, The molecular principles of gene regulation by Polycomb repressive complexes. *Nat. Rev. Mol. Cell Biol.* **22**, 815–833 (2021).

25. F. W. Schmitges, A. B. Prusty, M. Faty, A. Stutzer, G. M. Lingaraju, J. Aiwazian, R. Sack, D. Hess, L. Li, S. Zhou, R. D. Bunker, U. Wirth, T. Bouwmeester, A. Bauer, N. Ly-Hartig, K. Zhao, H. Chan, J. Gu, H. Gut, W. Fischle, J. Muller, N. H. Thoma, Histone methylation by PRC2 is inhibited by active chromatin marks. *Mol. Cell* **42**, 330–341 (2011).

26. W. Yuan, M. Xu, C. Huang, N. Liu, S. Chen, B. Zhu, H3K36 methylation antagonizes PRC2-mediated H3K27 methylation. *J. Biol. Chem.* **286**, 7983–7989 (2011).

27. K. Finogenova, J. Bonnet, S. Poepsel, I. B. Schafer, K. Finkl, K. Schmid, C. Litz, M. Strauss, C. Benda, J. Müller, Structural basis for PRC2 decoding of active histone methylation marks H3K36me2/3. *eLife* **9**, e61964 (2020).

28. E. Dorafshan, T. G. Kahn, A. Glotov, M. Savitsky, M. Walther, G. Reuter, Y. B. Schwartz, Ash1 counteracts Polycomb repression independent of histone H3 lysine 36 methylation. *EMBO Rep.* **20**, **e46762** (2019).

29. S. J. Elsaesser, A. D. Goldberg, C. D. Allis, New functions for an old variant: No substitute for histone H3.3. *Curr. Opin. Genet. Dev.* **20**, 110–117 (2010).

30. B. Loppin, F. Berger, Histone variants: The nexus of developmental decisions and epigenetic memory. *Annu. Rev. Genet.* **54**, 121–149 (2020).

31. A. Sakai, B. E. Schwartz, S. Goldstein, K. Ahmad, Transcriptional and developmental functions of the H3.3 histone variant in Drosophila. *Curr. Biol.* **19**, 1816–1820 (2009).

32. J. A. Kassis, J. L. Brown, Polycomb group response elements in *Drosophila* and vertebrates, in *Advances in Genetics* (Elsevier, 2013), pp. 83–118.

33. J. Muller, J. A. Kassis, Polycomb response elements and targeting of Polycomb group proteins in Drosophila. *Curr. Opin. Genet. Dev.* **16**, 476–484 (2006).

34. G. Streubel, A. Watson, S. G. Jammula, A. Scelfo, D. J. Fitzpatrick, G. Oliviero, R. McCole, E. Conway, E. Glancy, G. L. Negri, E. Dillon, K. Wynne, D. Pasini, N. J. Krogan, A. P. Bracken, G. Cagney, The H3K36me2 methyltransferase Nsd1 demarcates PRC2-mediated H3K27me2 and H3K27me3 domains in embryonic stem cells. *Mol. Cell* **70**, 371–379.e5 (2018).

35. Y. Zheng, S. M. Sweet, R. Popovic, E. Martinez-Garcia, J. D. Tipton, P. M. Thomas, J. D. Licht, N. L. Kelleher, Total kinetic analysis reveals how combinatorial methylation patterns are established on lysines 27 and 36 of histone H3. *Proc. Natl. Acad. Sci. U.S.A.* **109**, 13549–13554 (2012).

36. P. B. Talbert, S. Henikoff, Histone variants on the move: Substrates for chromatin dynamics. *Nat. Rev. Mol. Cell Biol.* **18**, 115–126 (2017).

37. A. S. Akhmanova, P. C. T. Bindels, J. Xu, K. Miedema, H. Kremer, W. Hennig, Structure and expression of histone H3.3 genes in Drosophila melanogaster and Drosophila hydei. *Genome* **38**, 586–600 (1995).

38. M. Hodl, K. Basler, Transcription in the absence of histone H3.3. *Curr. Biol.* **19**, 1221–1226 (2009).

39. M. Leatham-Jensen, C. M. Uyehara, B. D. Strahl, A. G. Matera, R. J. Duronio, D. J. McKay, Lysine 27 of replication-independent histone H3.3 is required for Polycomb target gene silencing but not for gene activation. *PLOS Genet.* **15**, e1007932 (2019).

40. S. E. Celniker, S. Sharma, D. J. Keelan, E. B. Lewis, The molecular genetics of the bithorax complex of Drosophila: cis-regulation in the Abdominal-B domain. *EMBO J.* **9**, 4277–4286 (1990).

41. N. Javeed, N. J. Tardi, M. Maher, S. Singari, K. A. Edwards, Controlled expression of Drosophila homeobox loci using theHostile takeoversystem. *Dev. Dyn.* **244**, 808–825 (2015).

42. U. Fresán, M. A. Rodríguez-Sánchez, O. Reina, V. G. Corces, M. L. Espinàs, Haspin kinase modulates nuclear architecture and Polycomb-dependent gene silencing. *PLOS Genet.* **16**, e1008962 (2020).

43. T. Furuyama, R. Banerjee, T. R. Breen, P. J. Harte, SIR2 is required for Polycomb silencing and is associated with an E(Z) histone methyltransferase complex. *Curr. Biol.* **14**, 1812–1821 (2004).

44. A. Lagarou, A. Mohd-Sarip, Y. M. Moshkin, G. E. Chalkley, K. Bezstarosti, J. A. Demmers, C. P. Verrijzer, dKDM2 couples histone H2A ubiquitylation to histone H3 demethylation during Polycomb group silencing. *Genes Dev.* **22**, 2799–2810 (2008).

45. R. P. Lifton, M. L. Goldberg, R. W. Karp, D. S. Hogness, The organization of the histone genes in Drosophila melanogaster: Functional and evolutionary implications. *Cold Spring Harb. Symp. Quant. Biol.* **42**(Pt 2), 1047–1051 (1978).

46. A. Chaouch, J. Berlandi, C. C. L. Chen, F. Frey, S. Badini, A. S. Harutyunyan, X. Chen, B. Krug, S. Hébert, A. Jeibmann, C. Lu, C. L. Kleinman, M. Hasselblatt, P. Lasko, M. Shirinian, N. Jabado, Histone H3.3 K27M and K36M mutations de-repress transposable elements through perturbation of antagonistic chromatin marks. *Mol. Cell* **81**, 4876–4890.e7 (2021).

47. C. Lu, S. U. Jain, D. Hoelper, D. Bechet, R. C. Molden, L. Ran, D. Murphy, S. Venneti, M. Hameed, B. R. Pawel, J. S. Wunder, B. C. Dickson, S. M. Lundgren, K. S. Jani, N. De Jay, S. Papillon-Cavanagh, I. L. Andrulis, S. L. Sawyer, D. Grynspan, R. E. Turcotte, J. Nadaf, S. Fahiminiyah, T. W. Muir, J. Majewski, C. B. Thompson, P. Chi, B. A. Garcia, C. D. Allis, N. Jabado, P. W. Lewis, Histone H3K36 mutations promote sarcomagenesis through altered histone methylation landscape. *Science* **352**, 844–849 (2016).

48. R. Popovic, E. Martinez-Garcia, E. G. Giannopoulou, Q. Zhang, Q. Zhang, T. Ezponda, M. Y. Shah, Y. Zheng, C. M. Will, E. C. Small, Y. Hua, M. Bulic, Y. Jiang, M. Carrara, R. A. Calogero, W. L. Kath, N. L. Kelleher, J. P. Wang, O. Elemento, J. D. Licht, Histone methyltransferase MMSET/NSD2 alters

EZH2 binding and reprograms the myeloma epigenome through global and focal changes in H3K36 and H3K27 methylation. *PLOS Genet.* **10**, e1004566 (2014).

49. P. J. Skene, J. G. Henikoff, S. Henikoff, Targeted in situ genome-wide profiling with high efficiency for low cell numbers. *Nat. Protoc.* **13**, 1006–1019 (2018).

50. G. A. Orsi, S. Kasinathan, K. T. Hughes, S. Saminadin-Peter, S. Henikoff, K. Ahmad, High-resolution mapping defines the cooperative architecture of Polycomb response elements. *Genome Res.* **24**, 809–820 (2014).

51. J. G. Henikoff, J. A. Belsky, K. Krassovsky, D. M. Macalpine, S. Henikoff, Epigenome characterization at single base-pair resolution. *Proc. Natl. Acad. Sci. U.S.A.* **108**, 18318–18323 (2011).

52. P. J. Skene, S. Henikoff, An efficient targeted nuclease strategy for high-resolution mapping of DNA binding sites. *eLife* **6**, e21856 (2017).

53. N. Nègre, C. D. Brown, L. Ma, C. A. Bristow, S. W. Miller, U. Wagner, P. Kheradpour, M. L. Eaton, P. Loriaux, R. Sealfon, Z. Li, H. Ishii, R. F. Spokony, J. Chen, L. Hwang, C. Cheng, R. P. Auburn, M. B. Davis, M. Domanus, P. K. Shah, C. A. Morrison, J. Zieba, S. Suchy, L. Senderowicz, A. Victorsen, N. A. Bild, A. J. Grundstad, D. Hanley, D. M. MacAlpine, M. Mannervik, K. Venken, H. Bellen, R. White, M. Gerstein, S. Russell, R. L. Grossman, B. Ren, J. W. Posakony, M. Kellis, K. P. White, A cis-regulatory map of the Drosophila genome. *Nature* **471**, 527–531 (2011).

54. J. Erceg, T. Pakozdi, R. Marco-Ferreres, Y. Ghavi-Helm, C. Girardot, A. P. Bracken, E. E. Furlong, Dual functionality of *cis*-regulatory elements as developmental enhancers and Polycomb response elements. *Genes Dev.* **31**, 590–602 (2017).

55. B. A. Bredesen, M. Rehmsmeier, DNA sequence models of genome-wide Drosophila melanogaster Polycomb binding sites improve generalization to independent Polycomb Response Elements. *Nucleic Acids Res.* **47**, 7781–7797 (2019).

56. T. Fiedler, M. Rehmsmeier, jPREdictor: A versatile tool for the prediction of cis-regulatory elements. *Nucleic Acids Res.* **34**, W546–W550 (2006).

57. L. Ringrose, M. Rehmsmeier, J.-M. Dura, R. Paro, Genome-wide prediction of Polycomb/trithorax response elements in Drosophila melanogaster. *Dev. Cell* **5**, 759–771 (2003).

58. J. Zeng, B. D. Kirk, Y. Gou, Q. Wang, J. Ma, Genome-wide polycomb target gene prediction in Drosophila melanogaster. *Nucleic Acids Res.* **40**, 5848–5863 (2012).

59. J. L. Brown, M.-A. Sun, J. A. Kassis, Global changes of H3K27me3 domains and Polycomb group protein distribution in the absence of recruiters Spps or Pho. *Proc. Natl. Acad. Sci. U.S.A.* **115**, E1839-E1848 (2018).

60. M. I. Kuroda, H. Kang, S. De, J. A. Kassis, Dynamic competition of polycomb and trithorax in transcriptional programming. *Annu. Rev. Biochem.* **89**, 235–253 (2020).

61. A. M. Deaton, M. Gómez-Rodríguez, J. Mieczkowski, M. Y. Tolstorukov, S. Kundu, R. I. Sadreyev, L. E. Jansen, R. E. Kingston, Enhancer regions show high histone H3.3 turnover that changes during differentiation. *eLife* **5**, e15316 (2016).

62. Y. Mito, J. G. Henikoff, S. Henikoff, Histone replacement marks the boundaries of cis-regulatory domains. *Science* **315**, 1408–1411 (2007).

63. A. Busturia, A. Lloyd, F. Bejarano, M. Zavortink, H. Xin, S. Sakonju, The MCP silencer of the Drosophila Abd-B gene requires both Pleiohomeotic and GAGA factor for the maintenance of repression. *Development* **128**, 2163–2173 (2001).

64. B. A. Horard, C. Tatout, S. Poux, V. Pirrotta, Structure of a polycomb response element and in vitro binding of polycomb group complexes containing GAGA factor. *Mol. Cell. Biol.* **20**, 3187–3197 (2000).

65. R. K. Mishra, J. Mihaly, S. P. Barges, A. Spierer, F. O. Karch, K. Hagstrom, S. E. Schweinsberg, P. Schedl, The iab-7 polycomb response element maps to a nucleosome-free region of chromatin and requires both GAGA and pleiohomeotic for silencing activity. *Mol. Cell. Biol.* **21**, 1311–1318 (2001).

66. A. Schwendemann, M. Lehmann, Pipsqueak and GAGA factor act in concert as partners at homeotic and many other loci. *Proc. Natl. Acad. Sci. U.S.A.* **99**, 12883–12888 (2002).

67. T. Nakayama, K. Nishioka, Y.-X. Dong, T. Shimojima, S. Hirose, Drosophila GAGA factor directs histone H3.3 replacement that prevents the heterochromatin spreading. *Genes Dev.* **21**, 552–561 (2007).

68. H. Okulski, B. Druck, S. Bhalerao, L. Ringrose, Quantitative analysis of polycomb response elements (PREs) at identical genomic locations distinguishes contributions of PRE sequence and genomic environment. *Epigenetics Chromatin* **4**, 4 (2011).

69. K. Ahmad, S. Henikoff, Histone H3 variants specify modes of chromatin assembly. *Proc. Natl. Acad. Sci. U.S.A.* **99**(Suppl 4), 16477–16484 (2002).

70. H.-T. Fang, C. A. El Farran, Q. R. Xing, L.-F. Zhang, H. Li, B. Lim, Y.-H. Loh, Global H3.3 dynamic deposition defines its bimodal role in cell fate transition. *Nat. Commun.* **9**, 1537 (2018).

71. E. McKittrick, P. R. Gafken, K. Ahmad, S. Henikoff, Histone H3.3 is enriched in covalent modifications associated with active chromatin. *Proc. Natl. Acad. Sci. U.S.A.* **101**, 1525–1530 (2004).

72. I. Bajusz, L. Sipos, Z. Gyorgypal, E. A. Carrington, R. S. Jones, J. Gausz, H. Gyurkovics, The Trithorax-mimic allele of Enhancer of zeste renders active domains of target genes accessible to polycomb-group-dependent silencing in Drosophila melanogaster. *Genetics* **159**, 1135–1150 (2001).

73. C. T. Wu, M. Howe, A genetic analysis of the Suppressor 2 of zeste complex of Drosophila melanogaster. *Genetics* **140**, 139–181 (1995).

74. I. A. Hernández-Romero, V. J. Valdes, De novo polycomb recruitment and repressive domain formation. *Epigenomes* **6**, 25 (2022).

75. R. K. Maeda, F. Karch, The ABC of the BX-C: The bithorax complex explained. *Development* **133**, 1413–1422 (2006).

76. R. J. Diederich, V. K. Merrill, M. A. Pultz, T. C. Kaufman, Isolation, structure, and expression of labial, a homeotic gene of the Antennapedia Complex involved in Drosophila head development. *Genes Dev.* **3**, 399–414 (1989).

77. M. P. Scott, A. J. Weiner, T. I. Hazelrigg, B. A. Polisky, V. Pirrotta, F. Scalenghe, T. C. Kaufman, The molecular organization of the Antennapedia locus of Drosophila. *Cell* **35**, 763–776 (1983).

78. C. Ballare, M. Lange, A. Lapinaite, G. M. Martin, L. Morey, G. Pascual, R. Liefke, B. Simon, Y. Shi, O. Gozani, T. Carlomagno, S. A. Benitah, L. Di Croce, Phf19 links methylated Lys36 of histone H3 to regulation of Polycomb activity. *Nat. Struct. Mol. Biol.* **19**, 1257–1265 (2012).

79. L. Cai, S. B. Rothbart, R. Lu, B. Xu, W. Y. Chen, A. Tripathy, S. Rockowitz, D. Zheng, D. J. Patel, C. D. Allis, B. D. Strahl, J. Song, G. G. Wang, An H3K36 methylation-engaging Tudor motif of polycomb-like proteins mediates PRC2 complex targeting. *Mol. Cell* **49**, 571–582 (2013).

80. C. A. Musselman, N. Avvakumov, R. Watanabe, C. G. Abraham, M. E. Lalonde, Z. Hong, C. Allen, S. Roy, J. K. Nunez, J. Nickoloff, C. A. Kulesza, A. Yasui, J. Cote, T. G. Kutateladze, Molecular basis for H3K36me3 recognition by the Tudor domain of PHF1. *Nat. Struct. Mol. Biol.* **19**, 1266–1272 (2012).

81. R. Cao, H. Wang, J. He, H. Erdjument-Bromage, P. Tempst, Y. Zhang, Role of hPHF1 in H3K27 methylation and Hox gene silencing. *Mol. Cell. Biol.* **28**, 1862–1872 (2008).

82. J. Choi, A. L. Bachmann, K. Tauscher, C. Benda, B. Fierz, J. Muller, DNA binding by PHF1 prolongs PRC2 residence time on chromatin and thereby promotes H3K27 methylation. *Nat. Struct. Mol. Biol.* **24**, 1039–1047 (2017).

83. K. Sarma, R. Margueron, A. Ivanov, V. Pirrotta, D. Reinberg, Ezh2 requires PHF1 to efficiently catalyze H3 lysine 27 trimethylation in vivo. *Mol. Cell. Biol.* **28**, 2718–2731 (2008).

84. A. Friberg, A. Oddone, T. Klymenko, J. Muller, M. Sattler, Structure of an atypical Tudor domain in the Drosophila Polycomb-like protein. *Protein Sci.* **19**, 1906–1916 (2010).

85. S. O'Connell, L. Wang, S. Robert, C. A. Jones, R. Saint, R. S. Jones, Polycomblike PHD fingers mediate conserved interaction with enhancer of zeste protein. *J. Biol. Chem.* **276**, 43065–43073 (2001).

86. F. Tie, J. Prasad-Sinha, A. Birve, A. Rasmuson-Lestander, P. J. Harte, A 1-megadalton ESC/E(Z) complex from Drosophila that contains polycomblike and RPD3. *Mol. Cell. Biol.* **23**, 3352–3362 (2003).

87. M. Nekrasov, T. Klymenko, S. Fraterman, B. Papp, K. Oktaba, T. Köcher, A. Cohen, H. G. Stunnenberg, M. Wilm, J. Müller, Pcl-PRC2 is needed to generate high levels of H3-K27 trimethylation at Polycomb target genes. *EMBO J.* **26**, 4078–4088 (2007).

88. L. A. Banaszynski, D. Wen, S. Dewell, S. J. Whitcomb, M. Lin, N. Diaz, S. J. Elsasser, A. Chapgier, A. D. Goldberg, E. Canaani, S. Rafii, D. Zheng, C. D. Allis, Hira-dependent histone H3.3 deposition facilitates PRC2 recruitment at developmental loci in ES cells. *Cell* **155**, 107–120 (2013).

89. B. Papp, J. Muller, Histone trimethylation and the maintenance of transcriptional ON and OFF states by trxG and PcG proteins. *Genes Dev.* **20**, 2041–2054 (2006).

90. J. van Arensbergen, S. Dussaud, C. Pardanaud-Glavieux, J. García-Hurtado, C. Sauty, A. Guerci, J. Ferrer, P. Ravassard, A distal intergenic region controls pancreatic endocrine differentiation by acting as a transcriptional enhancer and as a polycomb response element. *PLOS ONE* **12**, e0171508 (2017).

91. H. Lindehell, A. Glotov, E. Dorafshan, Y. B. Schwartz, J. Larsson, The role of H3K36 methylation and associated methyltransferases in chromosome-specific gene regulation. *Sci. Adv.* **7**, eabh4390 (2021).

92. K. J. Evans, N. Huang, P. Stempor, M. A. Chesney, T. A. Down, J. Ahringer, Stable Caenorhabditis elegans chromatin domains separate broadly expressed and developmentally regulated genes. *Proc. Natl. Acad. Sci. U.S.A.* **113**, E7020–E7029 (2016).

93. M. A. Willcockson, S. E. Healton, C. N. Weiss, B. A. Bartholdy, Y. Botbol, L. N. Mishra, D. S. Sidhwani, T. J. Wilson, H. B. Pinto, M. I. Maron, K. A. Skalina, L. N. Toro, J. Zhao, C.-H. Lee, H. Hou, N. Yusufova, C. Meydan, A. Osunsade, Y. David, E. Cesarman, A. M. Melnick, S. Sidoli, B. A. Garcia, W. Edelmann, F. Macian, A. I. Skoultchi, H1 histones control the epigenetic landscape by local chromatin compaction. *Nature* **589**, 293–298 (2021).

94. F. Bantignies, V. Roure, I. Comet, B. Leblanc, B. Schuettengruber, J. Bonnet, V. Tixier, A. Mas, G. Cavalli, Polycomb-dependent regulatory contacts between distant Hox loci in Drosophila. *Cell* **144**, 214–226 (2011).

95. P. Buchenau, J. Hodgson, H. Strutt, D. J. Arndt-Jovin, The distribution of polycomb-group proteins during cell division and development in Drosophila embryos: Impact on models for silencing. *J. Cell Biol.* **141**, 469–481 (1998).

96. C. Grimaud, F. Bantignies, M. Pal-Bhadra, P. Ghana, U. Bhadra, G. Cavalli, RNAi components are required for nuclear clustering of polycomb group response elements. *Cell* **124**, 957–971 (2006).

97. A. J. Saurin, C. Shiels, J. Williamson, D. P. Satijn, A. P. Otte, D. Sheer, P. S. Freemont, The human polycomb group complex associates with pericentromeric heterochromatin to form a novel nuclear domain. *J. Cell Biol.* **142**, 887–898 (1998).

98. C. J. Lin, M. Conti, M. Ramalho-Santos, Histone variant H3.3 maintains a decondensed chromatin state essential for mouse preimplantation development. *Development* **140**, 3624–3634 (2013).

99. Y. Wang, H. Long, J. Yu, L. Dong, M. Wassef, B. Zhuo, X. Li, J. Zhao, M. Wang, C. Liu, Z. Wen, L. Chang, P. Chen, Q.-F. Wang, X. Xu, R. Margueron, G. Li, Histone variants H2A.Z and H3.3 coordinately regulate PRC2-dependent H3K27me3 deposition and gene expression regulation in mES cells. *BMC Biol.* **16**, 107 (2018).

100. D. Arias Escayola, K. M. Neugebauer, Dynamics and function of nuclear bodies during embryogenesis. *Biochemistry* **57**, 2462–2469 (2018).

101. R. J. Duronio, W. F. Marzluff, Coordinating cell cycle-regulated histone gene expression through assembly and function of the Histone Locus Body. *RNA Biol.* **14**, 726–738 (2017).

102. J. E. Sleeman, L. Trinkle-Mulcahy, Nuclear bodies: New insights into assembly/dynamics and disease relevance. *Curr. Opin. Cell Biol.* **28**, 76–83 (2014).

103. K. M. Dorighi, J. W. Tamkun, The trithorax group proteins Kismet and ASH1 promote H3K36 dimethylation to counteract Polycomb group repression in Drosophila. *Development* **140**, 4182–4192 (2013).

104. Y. Tanaka, Z. Katagiri, K. Kawahashi, D. Kioussis, S. Kitajima, Trithorax-group protein ASH1 methylates histone H3 lysine 36. *Gene* **397**, 161–168 (2007).

105. S. Schmahling, A. Meiler, Y. Lee, A. Mohammed, K. Finkl, K. Tauscher, L. Israel, M. Wirth, J. Philippou-Massier, H. Blum, B. Habermann, A. Imhof, J. J. Song, J. Muller, Regulation and function of H3K36 di-methylation by the trithorax-group protein complex AMC. *Development* **145**, dev163808 (2018).

106. T. Klymenko, J. Muller, The histone methyltransferases Trithorax and Ash1 prevent transcriptional silencing by Polycomb group proteins. *EMBO Rep.* **5**, 373–377 (2004).

107. U. Gunesdogan, H. Jackle, A. Herzig, A genetic system to assess in vivo the functions of histones and histone modifications in higher eukaryotes. *EMBO Rep.* **11**, 772–776 (2010).

108. S. Kondo, R. Ueda, Highly improved gene targeting by germline-specific Cas9 expression in Drosophila. *Genetics* **195**, 715–721 (2013).

109. K. Ahmad, CUT&RUN with Drosophila tissues V.1., protocols.io (2018); dx.doi.org/10.17504/protocols.io.umfeu3n.

110. Y. Liao, G. K. Smyth, W. Shi, featureCounts: An efficient general purpose program for assigning sequence reads to genomic features. *Bioinformatics* **30**, 923–930 (2014).

111. M. I. Love, W. Huber, S. Anders, Moderated estimation of fold change and dispersion for RNA-seq data with DESeq2. *Genome Biol.* **15**, 550 (2014).

112. F. Ramírez, D. P. Ryan, B. Grüning, V. Bhardwaj, F. Kilpert, A. S. Richter, S. Heyne, F. Dündar, T. Manke, deepTools2: A next generation web server for deep-sequencing data analysis. *Nucleic Acids Res.* **44**, W160–165 (2016).

113. A. R. Quinlan, I. M. Hall, BEDTools: A flexible suite of utilities for comparing genomic features. *Bioinformatics* **26**, 841–842 (2010).

114. S. Andrews, FastQC: A quality control tool for high throughput sequence data (Babraham Institute, 2010).

115. S. W. Wingett, S. Andrews, FastQ screen: A tool for multi-genome mapping and quality control. *F1000Research* **7**, 1338 (2018).

116. B. Langmead, S. L. Salzberg, Fast gapped-read alignment with Bowtie 2. *Nat. Methods* **9**, 357–359 (2012).

117. P. Danecek, J. K. Bonfield, J. Liddle, J. Marshall, V. Ohan, M. O. Pollard, A. Whitwham, T. Keane, S. A. McCarthy, R. M. Davies, H. Li, Twelve years of SAMtools and BCFtools. *Gigascience* **10**, giab008 (2021).

118. W. J. Kent, A. S. Zweig, G. Barber, A. S. Hinrichs, D. Karolchik, BigWig and BigBed: Enabling browsing of large distributed datasets. *Bioinformatics* **26**, 2204–2207 (2010).

119. Y. Zhang, T. Liu, C. A. Meyer, J. Eeckhoute, D. S. Johnson, B. E. Bernstein, C. Nusbaum, R. M. Myers, M. Brown, W. Li, X. S. Liu, Model-based Analysis of ChIP-Seq (MACS). *Genome Biol.* **9**, R137 (2008).

120. M. N. Patwardhan, C. D. Wenger, E. S. Davis, D. H. Phanstiel, Bedtoolsr: An R package for genomic data analysis and manipulation. *J. Open Source Softw.* **4**, 1742 (2019).